applied sciences

MDPI

Article

Improvement of Intake Structures in a Two-Way Pumping Station with Experimental Analysis

Yanjun Li, Rong Lu *, Huiyan Zhang, Fanjie Deng and Jianping Yuan *

National Research Center of Pumps, Jiangsu University, Zhenjiang 212013, China; lyj782900@ujs.edu.cn (Y.L.); 2111511016@stmail.ujs.edu.cn (H.Z.); 2221811005@stmail.ujs.edu.cn (F.D.)

* Correspondence: 2111911005@stmail.ujs.edu.cn (R.L.); yh@ujs.edu.cn (J.Y.); Tel.: +86-139-1344-6553 (R.L.); +86-139-5280-1593 (J.Y.)

Received: 1 September 2020; Accepted: 27 September 2020; Published: 29 September 2020

Abstract: Pumping stations are important regulation facilities in a water distribution system. Intake structures can generally have a great influence on the operational state of the pumping station. To analyze the effects of the bell mouth height of the two-way intake on the performance characteristics and the pressure pulsations of a two-way pumping station, the laboratory-sized model pump units with three different intakes were experimentally investigated. To facilitate parameterized control, ellipse and straight lines were used to construct the profile of the bell mouth. The frequency domain and time-frequency domain of the pressure pulsations on the wall of intakes were analyzed by the Welch's power spectral density estimate and the continuous wavelet transform (CWT) methods, respectively. The results showed that the bell mouth height (H) has significant influences on the uniformity of the impeller inflow and the operation stability of the pump unit. When H = 204 mm, the data fluctuated greatly throughout the test process and the performance curves are slightly lower than the other two schemes. As the bell mouth height gradually decreases, the average pressure difference of each measuring point began to decrease, more homogeneous velocity distribution of impeller inflow can be ensured. The amplitude of blade passing frequency is obvious in the spectrum. While when (H) is more than 164 mm, the main frequency of pressure pulsations at three points fluctuates with the rotation of the impeller. When H decreases to 142 mm, pressure pulsations will be independent of the operating conditions and positions which contributes to the long-term stable operation of the pump unit.

Keywords: pumping stations; two-way intake; pressure pulsations; welch method; continuous wavelet transform

1. Introduction

Pumping stations play an important role in water resource allocation, agricultural irrigation and drainage, water environment improvement and urban flood fighting and drainage. As one kind of large-scale hydraulic engineering, the large costs of establishing, maintaining and operating pumping stations, particularly at a time of increasing energy costs, have motivated a search for improved design approaches and better operation of pumping stations [1–3]. Pumping stations with two-way inlet passages and two-way outlet passages possess functions of both diversion and drainage. Through the control of the gate, water can be transferred between upstream and downstream. However, this kind of pumping system has some disadvantages, such as low efficiency and easy to appear submerse vortex inflow passages, which may cause the unit vibration and does harm to the operating of pump unit [4,5]. Therefore, it is of great significance to study the internal flow phenomenon of the pumping station and then put forward the methods of restraining the unsteady flow to make the pumping stations operate safely and reliably.

The design of inlet and outlet areas of pumping stations significantly influences the overall cost of a pumping station not only in the design and construction phases but also during operation. Inhomogeneous inlet flow distribution due to an incorrectly shaped inlet geometry can cause serious flow problems and losses inside pump such as vortices and flow separation, which may affect the stability of the pump units. In order to predict hydropower intake flows with or without free-surface vortices, Akihiko et al. [6] applied large eddy simulation (LES) to solve this problem; the numerical results were generally consistent with the test. Helmut et al. [7] optimized intakes of several hydropower plants based on LES simulation; the results showed that the flow situation at the inflow is more homogeneous, which provides more stable inflow conditions for the impeller. Pei et al. [8] proposed a multi-objective optimization on the inlet pipe of a vertical inline pump based on genetic algorithm with an artificial neural network, and the results showed that the velocity distributions of outflow in the inlet pipe of the three optimized cases were more uniform than the original one; moreover, the hydraulic efficiency at different conditions were improved. Wang et al. [9] investigated the inflow characteristics of a canned nuclear coolant pump with different intakes; they found that the inflow field of the impeller becomes non-uniform by replacing the straight pipe with a channel head and the head and efficiency of the pump were reduced. This study indicates that the inlet distortion not only affects the external characteristics of the pump but also imposes an unbalanced force on the impeller, thus increasing the risk of fatigue failure of the impeller. Long et al. [10] numerically analyzed the inlet and outlet pressure pulsation characteristics of reactor coolant pumps with different inflows, the results show that the differences in both channel head and straight pipe inflows have significant effects on the unsteady pressure pulsation inside the pump.

Pressure and velocity pulsations are one of the main indicators of the stability of inflow. The stability of internal flow inside fluid machinery has been systematically investigated by several researchers. Choi et al. [11] made measurements of the fluctuating components of velocity and surface pressure with hot-wire probes and surface mounted pressure transducers on a seven bladed-back swept centrifugal water pump impeller operating with air as the working fluid. Then, the large-scale flow field instabilities in a pump rotor and the process of noise generation by these instabilities were elaborated. Guo et al. [12] conducted an experimental study on the pressure pulsations and impeller vibration in the centrifugal pump by using the diameter mode method. He concluded that when the circumferential pressure pulsation of impeller caused by rotor-stator interaction is not uniform, which can cause a kind of pitch diameter mode resonance of impeller. Spence et al. [13] investigated the effect of various geometry features on the pressure pulsations by Taguchi methods in a double suction pump; they concluded that the cutwater gap and vane arrangement are the two strongest influences on the pressure pulsation.

In this paper, the inlet flow field of the two-way pumping station was investigated, specifically focused on the impeller inflow. Considering that little research has been done on this kind of pumping station, this paper creatively optimizes the shape of the bell mouth of the two-way intake. Three different bell mouth heights were designed. The unsteady pressure at the outlet of intake were measured by the model test. The pressure fluctuation was analyzed via the Welch method and the continuous wavelet transform (CWT). The influence of bell mouth height on the pressure fluctuation and flow stability were analyzed. Finally, the inflow situation of the impeller was improved.

2. Overview of the Two-Way Pumping Station

Due to the different demands for water resources in different periods, the two-way pumping station was constructed to undertake the tasks of both drainage and diversion. Depending on the different water demands, the pumping station needs to transfer water between the two rivers. For example, when water needs to be transferred from river 1 to river 2, keep gate 1, 3 open and gate 2, 4 closed, and otherwise gate 2, 4 open and gate 1, 3 closed. The pumping station consists of six vertical axial flow pump units in total. Figure 1 is the elevation structure diagram of one pump unit. The pumping station is axisymmetric. The operating conditions are determined by the difference in water levels of

the rivers, which were obtained from the annual hydrologic statistics. The pumping station consists of six pump units with a total design flow of Q = 150 m^3/s and a total nominal power of P = 18 MW. Each unit consists of a vertical axial flow pump with a four-blade impeller and two-way flow passages. Table 1 shows the main parameters and operating conditions of the pumping station.

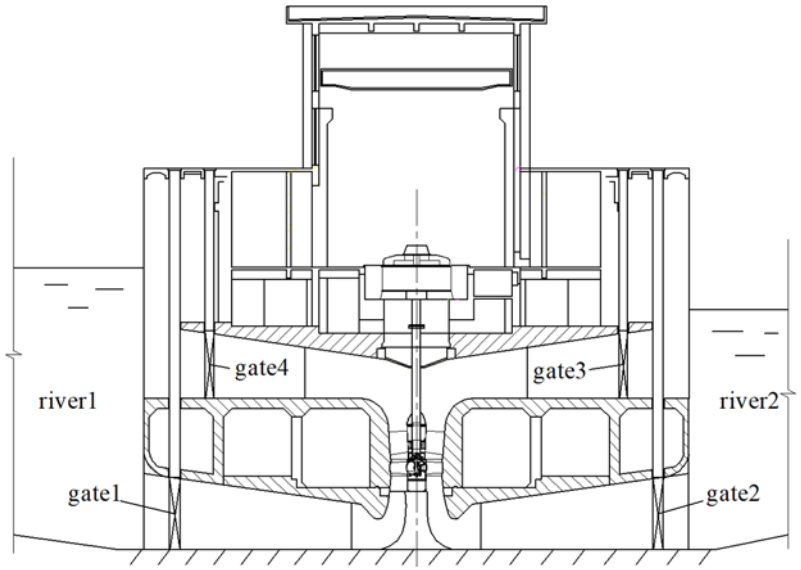

Figure 1. Profile of the pumping station.

Table 1. Main parameters and operating conditions of the pumping station.

Parameters	Values
Design flow Q	150 m^3/s
Impeller diameter D	2650 mm
Rotational speed n	150 r/min
Minimum head H_{min}	3.5 m
Design head H_d	4.7 m
Maximum head H_{max}	6.5 m

Since the units were brought into operation in 1991, it has created huge economic benefits. However, severe flooding occurred in 2016, and the units encountered serious problems such as blade breakage during the drainage process. The accident investigation showed that due to the unreasonable design of the intake, the impeller inflow was unstable, and the blades were subjected to alternating loads. The blades were prone to fatigue damage when operating under severe working conditions for a long time. Therefore, the optimization of the intake is of great significance to the safe and stable operation of the pumping station.

3. Overview of the Two-Way Pumping Station

In this section, the experimental setup of the pumping station model will be introduced in detail together with a brief introduction of the basic parameters of the pump unit, instruments and experimental procedures.

3.1. Main Parameters of the Test Model

The experiment was carried out on a laboratory-sized model pump unit. Figure 2 shows a three-dimensional perspective view of the investigated model pump unit. It is a vertically mounted axial flow pump unit which contains axial impeller, diffuser, two-way inlet and outlet passages. The cavitation and head performance of the axial flow pump are related to nD, in order to keep the cavitation

performance of the pump unit unchanged, when scaling the prototype, the principle of constant tip velocity (nD = constant) should be followed. The model pump impeller diameter D_M = 300 mm, then the zoom factor is D_M/D = 0.1132. The rotation speed of model pump $n_M = nD/D_M$ = 1325 r/min.

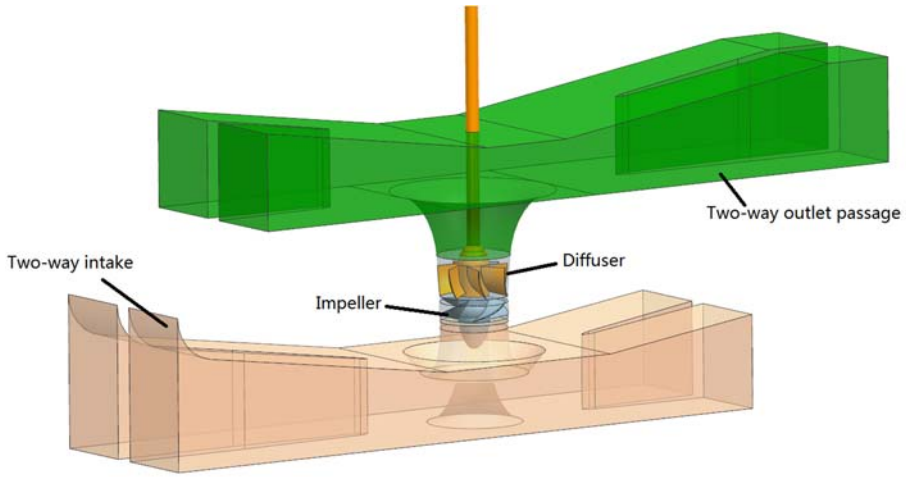

Figure 2. Three-dimensional perspective view of the model pump unit.

3.2. Test Schemes

Three intakes with different bell mouth heights were designed. For the intake, it contains a division pier, bell mouth and flow guide cone. The ellipse and straight lines were used to construct the profile of the bell mouth. A cartesian coordinate system is established at the center point of the impeller, which is the intersection point of the impeller centerline and the rotation axis, as is shown in Figure 3. The impeller centerline is the X-axis and rotation axis represents the Y-axis.

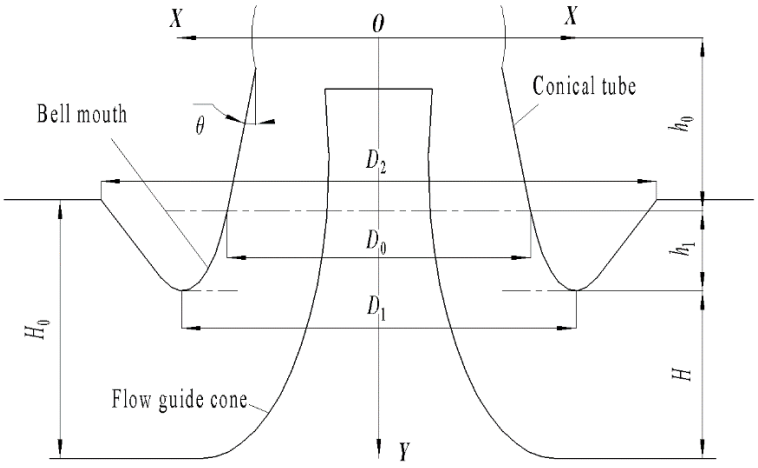

Figure 3. Schematic diagram of the bell mouth.

To facilitate the parameterized control of the profile, constraints were imposed on the ellipse, that is, the ellipse is tangent to the straight line at the inlet of the conical tube and the major axis is parallel to the rotation axis. Then, the bell mouth profile can be controlled by the following geometric relationship [14]:

Ellipse equation:

$$\frac{(x - D_1/2)}{a^2} + \frac{[y - (h_0 + h_1 - b)]^2}{b^2} = 1 \quad (1)$$

where a, b are the length of semi-minor axis and semi-major axis of the ellipse, respectively, h_0 is the distance from the inlet of the conical tube to the impeller centerline and h_1 is the distance from the inlet of the conical tube to the lowest point of the bell mouth.

According to Equation (1), the derivative of y is:

$$\frac{dy}{dx} = \frac{-b^2(x - D_1/2)}{a^2(y + b - h_0 - h_1)} \tag{2}$$

Referring to the proposed constraints:

$$\frac{-b^2(x - D_1/2)}{a^2(y + b - h_0 - h_1)} = \frac{1}{\tan\theta} \tag{3}$$

Substituting the coordinates of the tangent point into Equation (1):

$$\begin{cases} a = \frac{(D_1 - D_0)h_1 - 2h_1^2\tan\theta}{2}\sqrt{\frac{D_1 - D_0}{h_1^2(D_1 - D_0) - 4h_1^2\tan\theta}} \\ b = \frac{(D_1 - D_0)h_1 - 2h_1^2\tan\theta}{D_1 - D_0 - 4h_1\tan\theta} \end{cases} \tag{4}$$

When changing the height H, all other geometric parameters should remain constant, as is shown in Table 2. In this way, the a and b in Equation (4) can be solved and the profile of the bell mouth can be uniquely determined.

Table 2. The values of constants for the model.

Constants	Values
θ	5°
D_0	292 mm
D_1	420 mm
D_2	611 mm
H_0	306 mm
h_o	80 mm
$h_1 + H$	407 mm

In this study, three model intakes with different heights were investigated, namely, H = 204 mm (original scheme), H = 164 mm and H = 142 mm. The model passages are made of welded steel plate with surface coating to meet the requirements of roughness similarity (Figure 4).

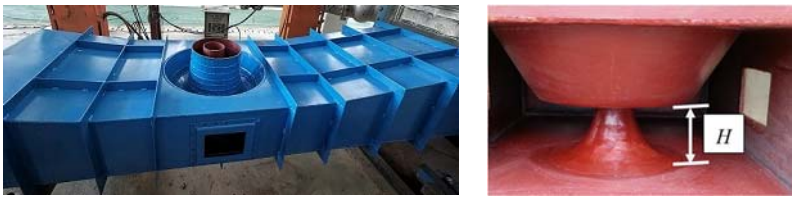

Figure 4. Photos of model intake.

3.3. Experimental System

A performance test of the pumping device with a laboratory-scale was conducted on the hydraulic four-quadrant test rig, Figure 5 describes the structural arrangement of the closed test loop facility, which is arranged vertically. The comprehensive permissible uncertainty of tested efficiency is better than ±0.3%. The pump device was vertically installed, and a DC motor is located above the shaft and provides power for the tested pump device, because the DC motor possesses better characteristics in starting and speed regulation; furthermore, this way it is less affected by electromagnetic interference.

A JCL2/500Nm torque meter with an accuracy of ±0.1% is installed between the shaft and motor to measure the shaft speed and power. The shaft penetrates the impeller hub and passes through the outtake and diffuser to transmit torque from the motor to the impeller. The intake and outtake are connected to the inlet and outlet water tanks, respectively, which can make the flow and water pressure steady. The outlet pipe is also connected with a booster pump, which is used to increase the flow rate when the head of the tested device is low. Valves adjust the pressure drop in the loop and consequently the operating condition. Flow rates are obtained by an electromagnetic flowmeter with an uncertainty of ±0.2%. The head is measured by the EJA intelligent differential pressure gauge connected to the inlet and outlet water tanks with a test range from 0–25 m; its uncertainty is better than ±0.1%. EJA represents a family of differential pressure gauges. The type used in this paper is EJA 110A.

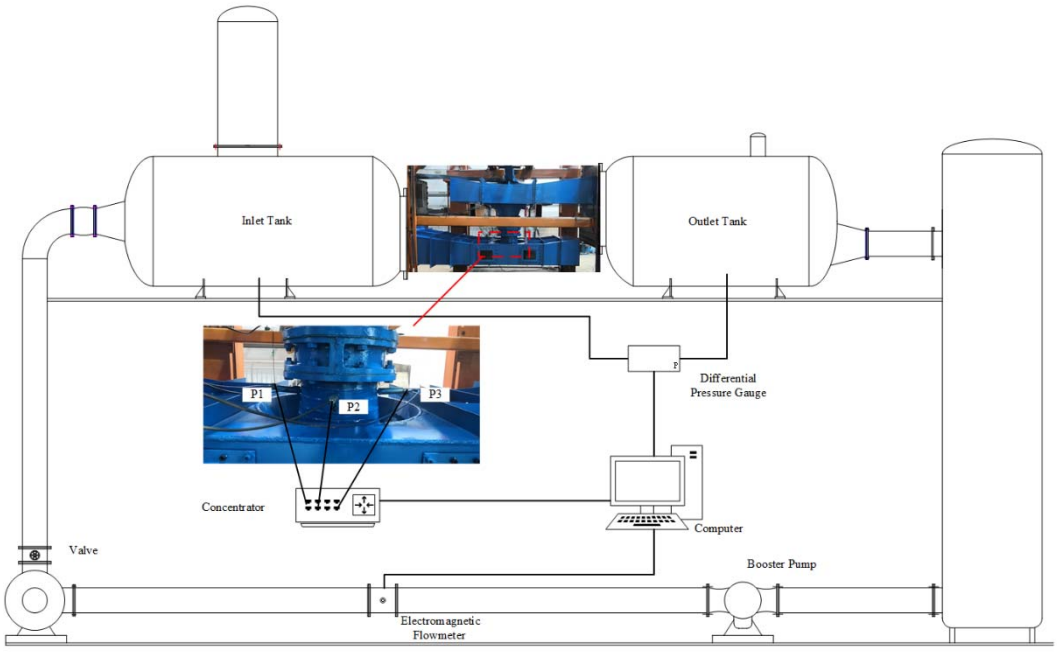

Figure 5. Schematic diagram of closed test rig.

A high precision digital pressure acquisition system is used to measure the unsteady pressure signals near the outlet of the intakes. Three dynamic pressure transducers (CY200) were arranged just 10 cm upstream of the inlet of the impeller. They were placed flush with the wall of the shrink tube, the circumferential angle between two adjacent sensors is 90 degrees. This kind of pressure transducer integrates the SOC (single-chip microcomputer system) chip and piezoresistive silicon crystal, makes full use of the processing and storage capacity of the microprocessor, and realizes the filtering, amplification, A/D conversion, correction and other functions of the pressure signal picked up by sensitive components. The pressure signal can be directly output as digital signals that can be displayed and stored. The comprehensive precision of the pressure transducer is 0.1%. The sampling frequency fs was set as 1000 Hz and the data was sampled for 20 s after the pump reached a stable operating point. The analyzed frequency is within the range 0–441.7 Hz, which meets the requirement of the Nyquist sampling theorem.

Figure 6 shows a schematic view of the tested configuration with the reference marks of the measurement positions:

- P1 and P3 are located on the symmetrical plane of the intake. P1 is close to the direction of inflow.
- P2 is located on the vertical plane of the symmetrical surface of the intake.

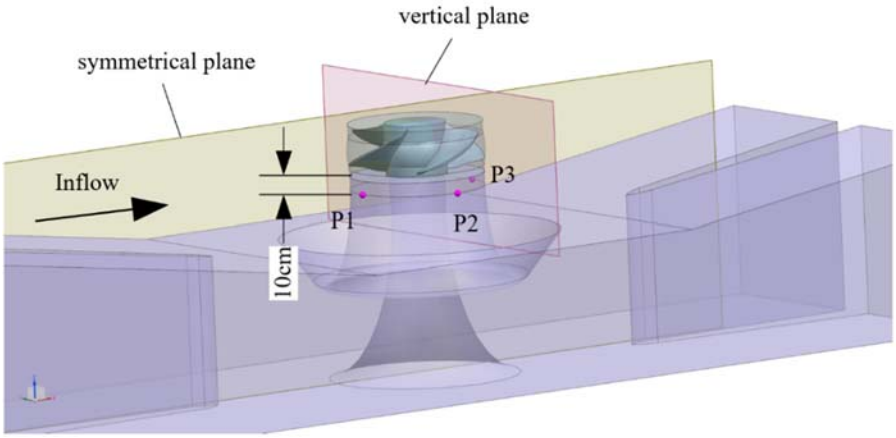

Figure 6. Distribution of pressure monitors.

4. Data Process Methods

4.1. Spectral Analysis Method

The Welch method was used to obtain the frequency domain of the power spectrum density (PSD) of the pressure pulsations by averaging the estimates of each segment. First, the finite-duration signal $x(n)$ is further subdivided into K (possibly overlapping) segments of length L and a data window is selected to intercept the signal; then, the PSD estimation of each segment was calculated as followed [15]:

$$P_L^i(f) = \frac{1}{LU}\left|\sum_{n=0}^{L-1} x_i(n) \times w(n) \times e^{-j2\pi fn}\right|^2, i = 1,2 \ldots K \quad (5)$$

where $w(n)$ is a data window, and U is written as [16]:

$$U = \frac{1}{L}\sum_{n=0}^{L-1} w^2(n) \quad (6)$$

The power spectrum estimation is given by averaging the periodograms from the K segments [17]:

$$P(f) = \frac{1}{K}\sum_{i=1}^{K} P_L^i(f) \quad (7)$$

In this study, the Hanning window function was applied to avoid aliasing and spectral leakage. Each time series signal was divided into eight signal segments with overlapping samples whose lengths were 50% that of each segment. The one-sided PSD over the frequency ranges specified for input series $x(n)$ was computed.

4.2. Time-Frequency Analysis Method

The signal processing in the frequency domain allows finding and analyzing the spectral components contained in the whole-time domain, but it does not allow an assignment of these spectral components to time. Time-frequency analysis has been proved to be suitable for analyzing non-stationary signals, especially when the signal is corrupted by transients. The appearance and disappearance of these transients often have physical significance. Therefore, it is important to be able to localize these transients in addition to characterizing oscillatory components in the signal. The wavelet transform is a linear transform that uses a series of oscillating functions with different frequencies as window functions. When at high frequencies, the wavelet reaches a high time resolution but a low-frequency resolution, whereas at low frequencies, a low time resolution and a high-frequency

resolution are achieved, which makes them more suitable for non-stationary signal analysis. For this purpose, the one-dimensional continuous wavelet transform (CWT) of the discrete sampled pressure signal was computed to determine the continuity in time [18]:

$$C\langle a, b; f(t), \psi(t)\rangle = \frac{1}{\sqrt{a}}\int_{-\infty}^{\infty} f(t)\psi^*\left(\frac{t-b}{a}\right)dt \tag{8}$$

where $\psi\left(\frac{t-b}{a}\right)$ is the wavelet function at the scale dilation a (a∈R+) and translation b (b∈R) of the mother wavelet function $\psi(t)$. The asterisk (*) represents the complex conjugate.

In practice, the constant signal is often obtained by the discrete sampling data $x(j)$ $j = 1, 2, \ldots M$, where M is number of samples of signal, Thus, the discretized variant of CWT can be redefined as [19]:

$$W = \sum_{j=1}^{M} x(j)\frac{1}{\sqrt{a}}\psi^*\left[\frac{(j-b)}{a}\right] \tag{9}$$

In this research, the complex Morlet wavelet was chosen, since it provided a good balance between the time and frequency localization and it returned information about both amplitude and phase. The complex Morlet wavelet both in time and frequency domain are mathematically defined as [20]:

$$\psi(t) = \frac{1}{\sqrt{\pi f_b}}e^{j2\pi f_c(t-t^2/f_b)} \tag{10}$$

$$\psi(f) = e^{-\pi^2 f_b(f-f_c)^2} \tag{11}$$

where f_c is the wavelet center frequency and f_b is the bandwidth parameter is the inverse of the variance in frequency, Therefore, increasing f_b results in a narrower concentration of energy around the center frequency. In this research, f_c and f_b were all taken to be 3 (cmor3-3), which can approximately satisfy the condition admissibility. Figure 7 showss the image of the cmor3-3.

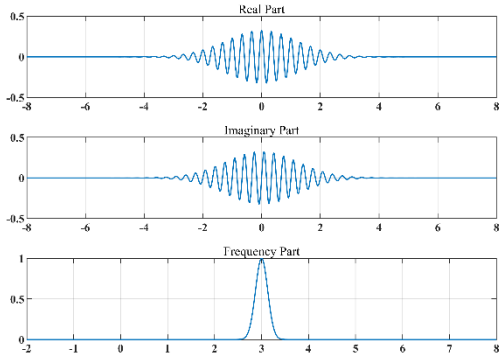

Figure 7. Complex Morlet wavelet with $f_b = f_c = 3$.

5. Results and Discussions

5.1. Comparison of Performance Curves for Three Intakes

Figure 8 shows a comparison of the performance curves of the axial flow pump unit with three different intakes. It can be seen from Figure 8a that the head curves are nearly the same; the head under partial load conditions increase when H is reduced. However, when H = 204 mm, the data fluctuated greatly throughout the test process. The inner flow consistently exhibited unstable patterns. Moreover, the head curve is slightly lower than the other two schemes. As H decreases, data oscillation is improved, and the operation of the unit gradually tends to be stable under various working conditions. Figure 8b compares the efficiency curves for the three intakes mentioned above. For H = 204 mm,

the unstable inflow reduces impeller efficiency, so the pump unit efficiency is the lowest. When H is further reduced to 142 mm, the flow at the impeller inlet is more stable and the impeller efficiency should be higher. However, the fluid resistance loss of the bell mouth increases, resulting in the efficiency of the pump set being unchanged.

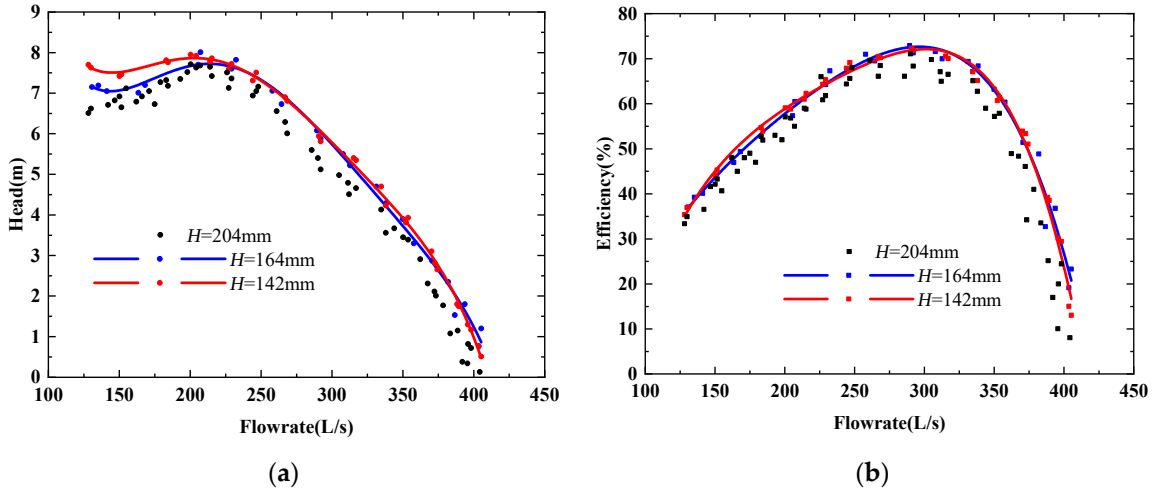

(**a**) (**b**)

Figure 8. Comparison of performance curves: (**a**) Head curves; (**b**) Efficiency curves.

5.2. Comparison of Pressure Values at Different Measuring Positions

The intake provides inflow for the pump impeller. The uniformity of the inflow velocity of the impeller not only affects the hydraulic performance of the pump but also determines the stability of the pump unit. Therefore, the uniformity of the impeller inflow velocity is one of the important indicators for evaluating the performance of the intake. The total pressure of the test flow can be regarded as Table 1 atm. According to the Bernoulli equation, the sum of the pressure energy and the kinetic energy of the same height should be the same. Therefore, the uniformity of the inflow velocity of the impeller can be obtained by the pressure distribution. Figure 9 shows the time-domain of pressure signals. By comparison of pressure values of different schemes, the bell mouth height has a significant influence on the uniformity of inflow of the impeller. When H is 204 mm, there is a big difference in the average pressure at the three measuring points. It indicates that the intake outlet velocity shows serious inhomogeneous distribution under all working conditions, most of the fluid easily enters the impeller directly from the side close to the inflow, resulting in the highest flow velocity at P1, which shows the lowest pressure; since it is difficult for the fluid to bypass the flow guide cone to the other side, P3 has the lowest flow rate and the highest pressure; the blades were subjected to alternating loads, and the blades were prone to fatigue damage under this condition for a long time. As the bell mouth height gradually decreases, the average pressure difference of each measuring point began to decrease, the fluid cannot easily enter the impeller directly from the side close to the inflow and more fluid enters the impeller more evenly around the guide cone; when the bell mouth height is reduced to 142 mm, the average pressure of each measuring point is almost the same, which means that the intake can provide the most uniform inflow conditions for the impeller. It is conducive to the long-term stable operation of the pump unit.

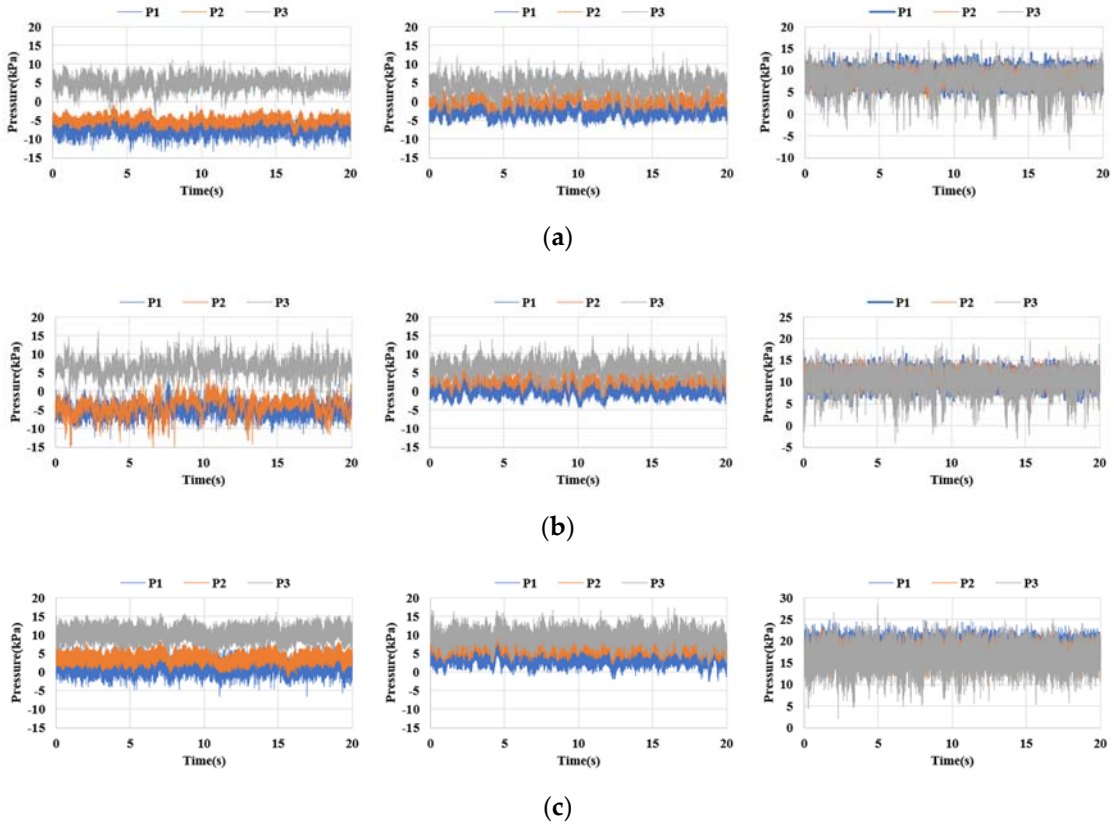

Figure 9. Time domain of pressure pulsations for three schemes at different conditions: (**a**) H_{min} = 3.5m; (**b**) H_d = 4.7 m; (**c**) H_{max} = 6.5 m (each row from left to right is H = 204 mm, 164 mm and 142 mm).

5.3. Pressure Pulsations under Low Head Condition

Figure 10 shows a comparison of the PSD of the unsteady pressure, measured in the intake (P1–P3) versus the Strouhal number (St), a non-dimensional frequency based on the blade passing frequency (BPF). It is obvious that impeller rotation causes a pronounced periodic pressure pulsation system. There are two obvious peaks in the spectra: the main one at St = 1 and the second one at St = 0.25 (rotation frequency, RF). All other peaks occur at a multiplier of these fluctuations. By comparing the pressure signals at different measuring points, the pressure amplitude gradually increases from P1 to P3, which means the flow field on the side away from the inflow is more prone to be instability. For H = 204 mm and H = 164 mm, there are large amplitudes between St = 0 and St = 0.25; the main frequencies at the three measuring points are different. The impeller inflow is severely uneven. For H = 142 mm, the main frequencies are all BPF at three measuring points, thus, the impeller inflow is more homogeneous. The peaks in frequency domain means that the blade number dominant the pressure pulsations in the intake for axial flow pump. Due to the asymmetry of the rotor in the circumferential direction, the peaks caused by rotational frequency is still obvious.

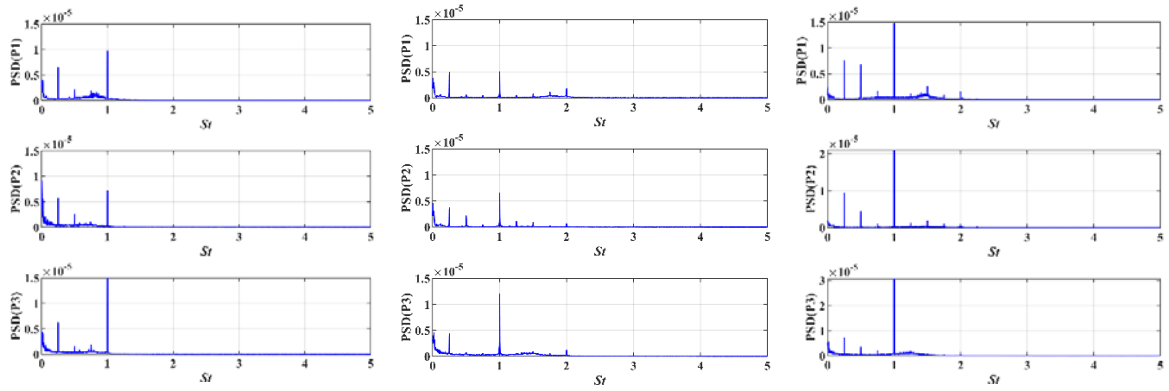

(**a**) (**b**) (**c**)

Figure 10. Frequency domain of pressure pulsations for three schemes at H_{min} = 3.5 m: (**a**) H = 204 mm; (**b**) H = 164 mm; (**c**) H = 142 mm.

The time-frequency domain analysis can identify unstable components in the dynamic pressure signals. Figure 11 shows the time-frequency domain of the pressure pulsations of three monitors. For H = 204 mm, discontinuous amplitudes are observed at P1and P3 in St = 0.75, the main frequency of the pressure signals fluctuate within the impeller rotation, there are large fluctuations in amplitudes of BPF. The pressure fluctuations consistently exhibited unsteady patterns. As the bell mouth height decreases, the amplitude of the discontinuous signals (St = 0.75) decreases significantly. However, discontinuous amplitudes in higher frequency gradually strengthen, but the main frequency of each measuring point tends to stabilize. When H = 142 mm, despite the amplitudes of BPF are the largest, the magnitudes are the most stable.

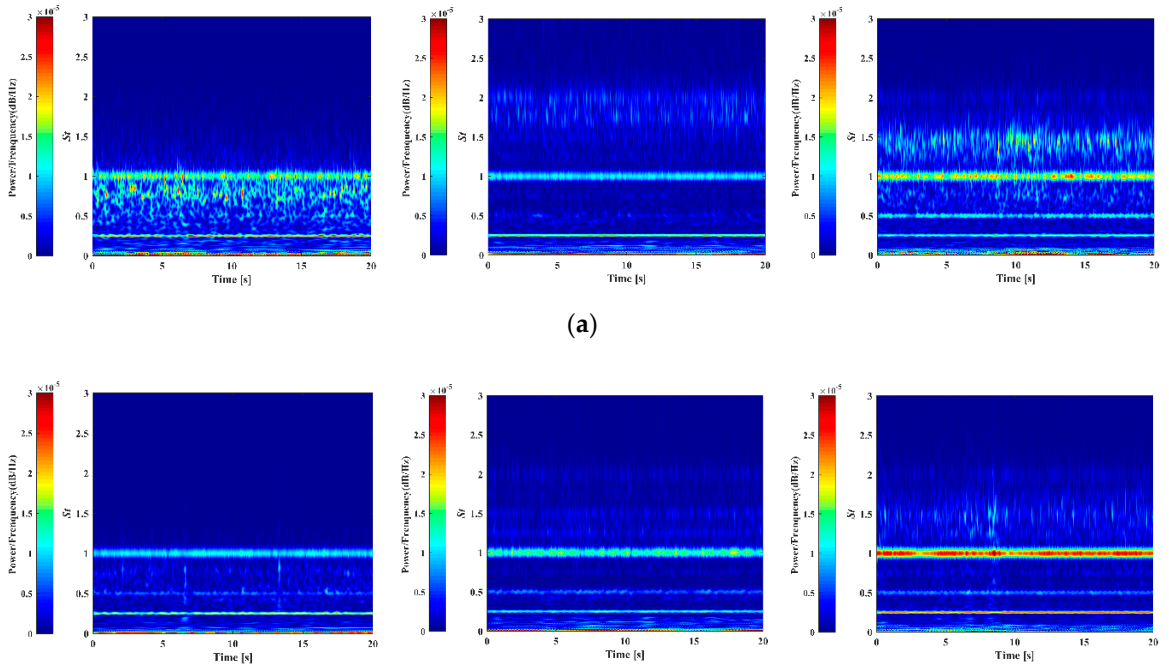

(**a**)

(**b**)

Figure 11. *Cont.*

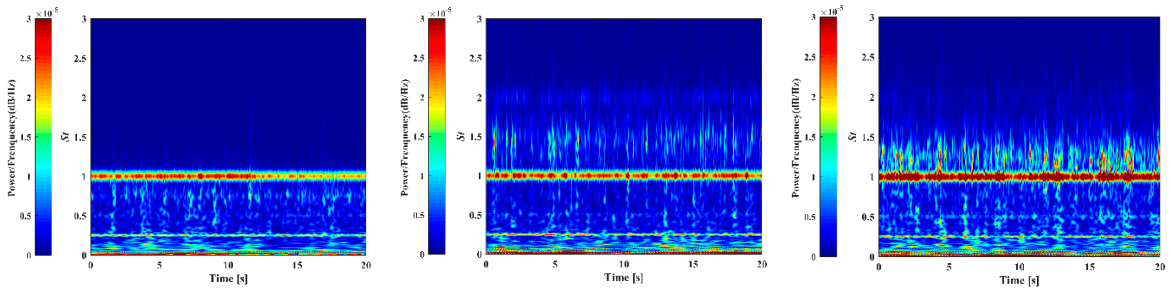

(**c**)

Figure 11. Time-frequency domain of pressure pulsations for three schemes at H_{min} = 3.5 m: (**a**) P1; (**b**) P2; (**c**) P3 (Each row from left to right is H = 204 mm, 164 mm and 142 mm).

5.4. Pressure Pulsations under Design Head Condition

Figure 12 illustrates the spectrum domain of the pressure pulsations at three monitors under the design condition. When H = 204 mm, the amplitudes of BPF and low frequency at three monitors increase significantly. Low frequency dominated the frequency domain of the pressure pulsations at P2, while the main frequency is BPF both at P1 and P3. The amplitude of P1 exceeds that of P3, the pressure pulsation law is changed compared with partial load conditions.

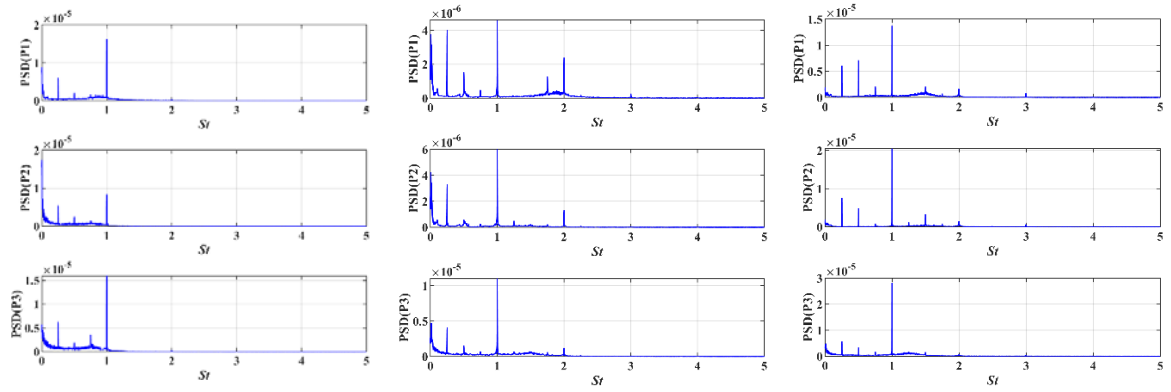

(**a**) (**b**) (**c**)

Figure 12. Frequency domain of pressure pulsations for three schemes at H_d = 4.7 m: (**a**) H = 204 mm; (**b**) H = 164 mm; (**c**) H = 142 mm.

The time-frequency domains of pressure pulsations in Figure 13 are like that of partial load conditions. When H = 204 mm, there are large discontinuous amplitudes between St = 0 and St = 1. The main frequency at P2 has a sudden change between St = 0 and St = 0.75. As the H decreases, the high frequency discontinuous signals begin to highlight.

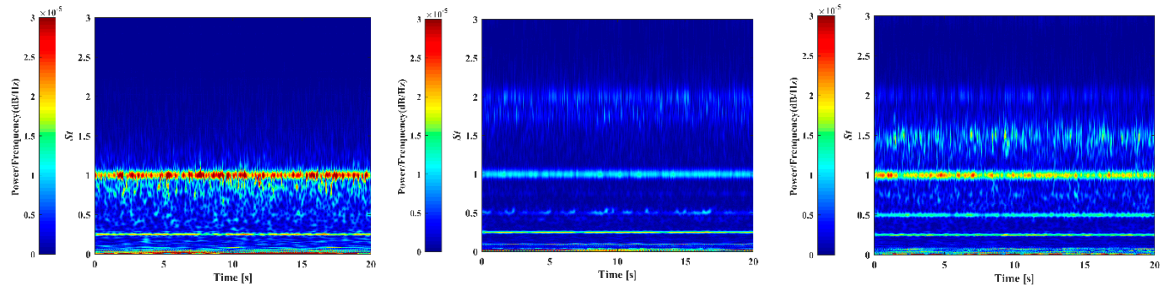

(**a**)

Figure 13. *Cont.*

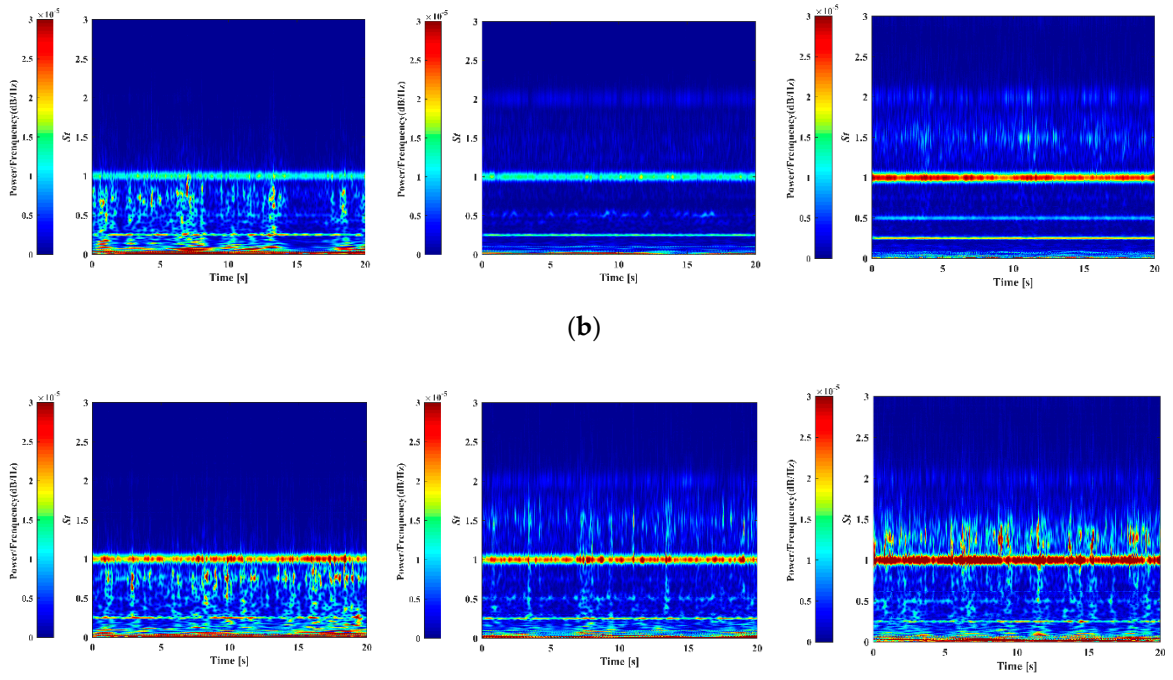

Figure 13. Time-frequency domain of pressure pulsations for three schemes at H_d = 4.7 m: (**a**) P1; (**b**) P2; (**c**) P3 (Each row from left to right is H = 204 mm, 164 mm and 142 mm).

5.5. Pressure Pulsations under High Head Condition

Practice has proved that pumping stations are prone to failures under high head conditions. Therefore, the stability of the inflow under high head conditions is extremely important to the safe operation of the pump unit. Figure 14 shows a comparison of the frequency domain of the pressure pulsations at three monitors under high head condition. It can be found that the amplitudes of the main frequency increase noticeably compared with the design condition. The blade number still dominated the pressure pulsations. As H decreases, amplitudes can be easily noticed in higher frequency ranges ($St > 1$). The main frequency for H = 164 mm at P1 is twice the BPF, while the main frequency in other cases is BPF.

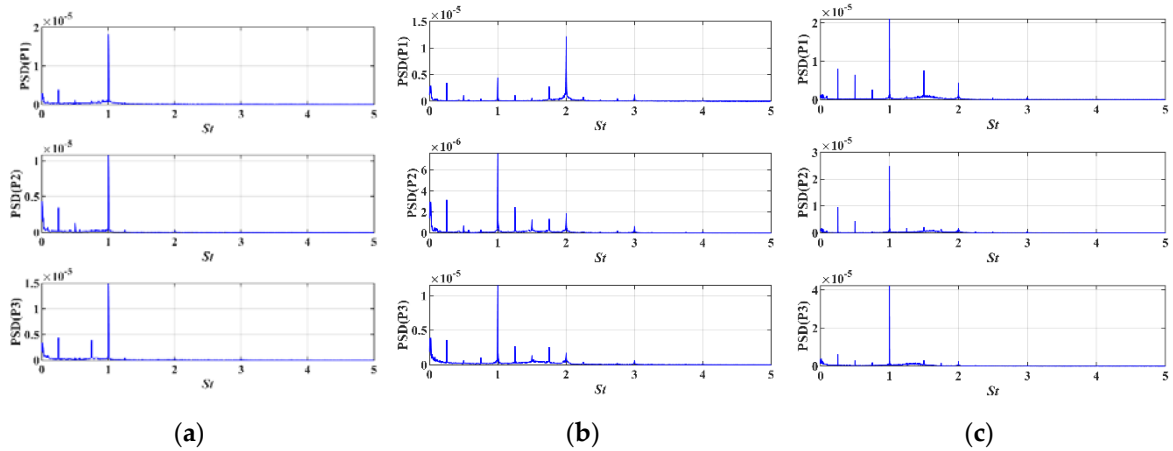

Figure 14. Frequency domain of pressure pulsations for three schemes at H_{max} = 6.5 m: (**a**) H = 204 mm; (**b**) H = 164 mm; (**c**) H = 142 mm.

The time-frequency domain of pressure pulsations in Figure 15 shows that the amplitude (St = 2) at P1 for H = 164 mm is discontinuous, which causes the main frequency of the pressure to fluctuate. As the impeller rotates, the blades are subjected to fluid forces of different frequencies. Under the action of alternating loads, the blades and the bearings are prone to fatigue damage, which reduces the stability and life of the unit.

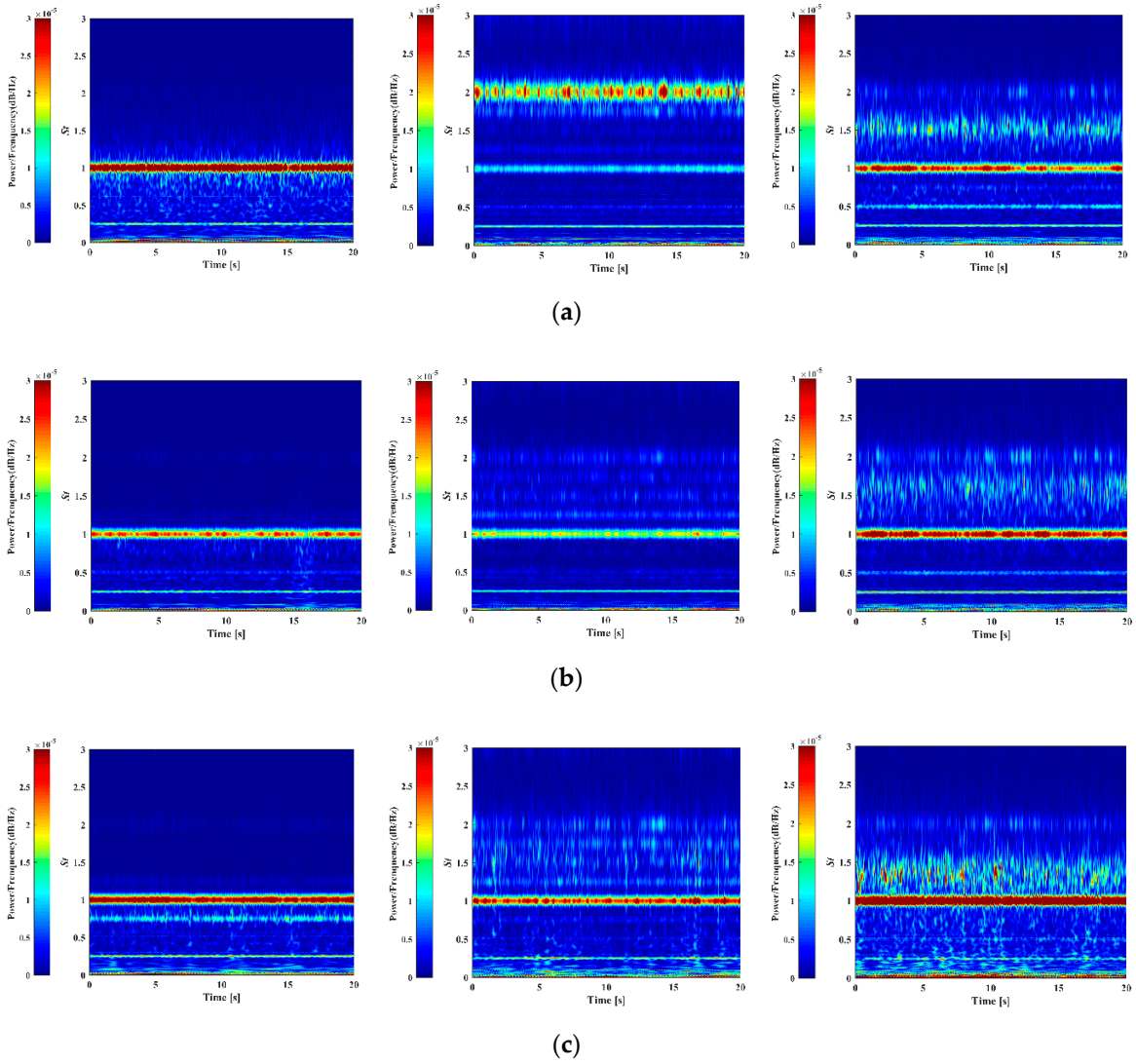

Figure 15. Time-frequency domain of pressure pulsations for three schemes at H_{max} = 6.5 m: (**a**) P1; (**b**) P2; (**c**) P3 (Each row from left to right is H = 204 mm, 164 mm and 142 mm).

In brief, due to the uneven impeller inflow conditions, the pressure pulsation law is greatly influenced by the positions and working conditions when H is 204 mm and 164 mm. However, for H = 142 mm, the main frequency of pressure pulsation at each measuring points is BPF and the amplitude is always continuous which can provide the most stable inflow for impeller. Therefore, to achieve the purpose of stable operation of the pumping station, the intake with H = 142 mm was chosen for the optimized scheme. It can be concluded that the two-way intake has important effects on the performance of the pumping unit and the above results can provide guidance for the design of two-way pumping station. The proposed methods can effectively reveal the internal flow mechanism and improve the internal flow phenomenon in hydraulic components and can be applied in other hydraulic engineering around the world.

6. Conclusions

Experimental tests were carried out to investigate the effects of the bell mouth height of intake on the performance curves and the unsteady pressure pulsations in a two-way pumping station. The methods of spectrum analysis and time-frequency analysis were applied to illustrate the pressure pulsation characteristics induced by the intake structures in the two-way pumping station. The conclusions drawn from the experimental investigations are summarized as follows:

(1) The bell mouth height has significant influence on the uniformity of the impeller inflow and the operation stability of the pump unit. The operation conditions of the pump unit are prone to instability when the bell mouth height is inappropriate, which affects the performance of the pump.
(2) The average pressure at different positions can reflect the impeller inflow velocity distribution. As the bell mouth height decreases, more uniform impeller inflow can be ensured.
(3) The RF and BPF are obvious in the spectra. The bell mouth height has an impact on the spectrum distribution. As the height decreases, the high-frequency amplitudes ($St > 1$) gradually increase.
(4) CWT can be used to analyze the variation of pressure pulsations with time. When H is 204 mm and 164 mm, discontinuous signals can be found between $St = 0$ and $St = 1$. Moreover, the main frequency is significantly affected by the positions and operating conditions. As H decreases further, the high frequency discontinuous signals begin to highlight, but pressure pulsations are independent of the operating conditions and positions which contributes to the long-term stable operation of the pump unit. This method can also be applied to the diagnosis of other signals in the pump station, such as vibration and noise, which are important indexes for the operation stability of the pumping station.

Author Contributions: Methodology, Y.L. and R.L.; experiment, Y.L.; analyzed the data, R.L. and H.Z.; writing—review and editing, Y.L. and F.D.; funding acquisition and validation, J.Y. All authors have read and agreed to the published version of the manuscript.

Funding: This research was funded by the Institute of Fluid Engineering Equipment, Natural Science Foundation of Jiangsu Province (Grant No. BK20180879), High-level Talent Research Foundation of Jiangsu University (Grant No. 18JDG012), National Key Research and Development Plan Project (Grant No. 2018YFB0606103) and Construction of Dominant Disciplines in Colleges and Universities and Universities in Jiangsu (PAPD).

Conflicts of Interest: The authors declare no conflict of interest.

References

1. Lei, X.; Tian, Y.; Zhang, Z.; Wang, L.; Xiang, X.; Wang, H. Correction of pumping station parameters in a one-dimensional hydrodynamic model using the Ensemble Kalman filter. *J. Hydrol.* **2019**, *568*, 108–118.
2. Zhang, F.; Appiah, D.; Hong, F.; Zhang, J.; Yuan, S.; Adu-Poku, K.A.; Wei, X. Energy loss evaluation in a side channel pump under different wrapping angles using entropy production method. *Int. Commun. Heat Mass Transf.* **2020**, *113*, 104526.
3. Wang, Y.; Zhang, F.; Yuan, S.; Chen, K.; Wei, X.; Appiah, D. Effect of URANS and Hybrid RANS-Large Eddy Simulation Turbulence Models on Unsteady Turbulent Flows Inside a Side Channel Pump. *ASME J. Fluids Eng.* **2020**, *142*, 061503.
4. Zhu, J.; Zeng, F. Experimental study on two-way flow passages in pumping system. *J. Mech. Sci. Technol.* **2008**, *22*, 1966–1970.
5. Liu, C.; Jin, Y.; Zhou, J.; Tang, F. Numerical simulation and experimental study of a two-floor structure pumping system. In Proceedings of the Power Conference, Palm Springs, CA, USA, 21–25 February 2010.
6. Nakayama, A.; Hisasue, N. Large eddy simulation of vortex flow in intake channel of hydropower facility. *J. Hydraul. Res.* **2010**, *48*, 415–427.
7. Benigni, H.; Schiffer, J.; Hoeller, S.; Jaberg, H. Improvement of intake structures with numerical simulation. In *World Congress ICOLD 2018*; Verlag der Technischen Universität Graz: Graz, Austria, 2018.

8. Pei, J.; Gan, X.; Wang, W.; Yuan, S.; Tang, Y. Multi-objective shape optimization on the inlet pipe of a vertical inline pump. *J. Fluids Eng.* **2019**, *141*, 061108.
9. Wang, Y.; Wang, P.; Tan, X.; Xu, Z.; Ruan, X. Research on the non-uniform inflow characteristics of the canned nuclear coolant pump. *Ann. Nucl. Energy* **2018**, *115*, 423–429.
10. Yun, L.; Dezhong, W.; Junlian, Y.; Hongjuan, R. Numerical investigation on the unsteady characteristics of reactor coolant pumps with non-uniform inflow. *Nucl. Eng. Des.* **2017**, *320*, 65–76.
11. Choi, J.-S.; McLaughlin, D.K.; Thompson, D.E. Experiments on the unsteady flow field and noise generation in a centrifugal pump impeller. *J. Sound Vib.* **2003**, *263*, 493–514.
12. Guo, S.; Maruta, Y. Experimental investigations on pressure fluctuations and vibration of the impeller in a centrifugal pump with vaned diffusers. *JSME Int. J. Ser. B Fluids Therm. Eng.* **2005**, *48*, 136–143.
13. Spence, R.; Amaral-Teixeira, J. A CFD parametric study of geometrical variations on the pressure pulsations and performance characteristics of a centrifugal pump. *Comput. Fluids* **2009**, *38*, 1243–1257.
14. Pei, J.; Meng, F.; Li, Y.; Yuan, S.; Chen, J. Fluid–structure coupling analysis of deformation and stress in impeller of an axial-flow pump with two-way passage. *Adv. Mech. Eng.* **2016**, *8*, 1687814016646266.
15. Wang, W.; Pei, J.; Yuan, S.; Yin, T. Experimental investigation on clocking effect of vaned diffuser on performance characteristics and pressure pulsations in a centrifugal pump. *Exp. Therm. Fluid Sci.* **2018**, *90*, 286–298.
16. Mateo, C.; Talavera, J.A. Short-Time Fourier Transform with the Window Size Fixed in the Frequency Domain (STFT-FD): Implementation. *SoftwareX* **2018**, *8*, 5–8.
17. Mateo, C.; Talavera, J.A. Short-time Fourier transform with the window size fixed in the frequency domain. *Digit. Signal Process.* **2018**, *77*, 13–21.
18. Pavesi, G.; Cavazzini, G.; Ardizzon, G. Time–frequency characterization of the unsteady phenomena in a centrifugal pump. *Int. J. Heat Fluid Flow* **2008**, *29*, 1527–1540.
19. Su, B.; Yin, Y.; Li, S.; Guo, Z.; Wang, Q.; Lin, M. Wavelet analysis on the turbulent flow structure of a T-junction. *Int. J. Heat Fluid Flow* **2018**, *73*, 124–142.
20. Wang, G.F.; Wang, T.Y.; Ren, C.; Li, H.W. Application of complex shifted morlet wavelet in vibration monitoring of spindle bearing of crank shaft grinder. In *Key Engineering Materials*; Trans Tech Publications: Zürich, Switzerland, 2004.